APL Materials

Accelerated carrier recombination by grain boundary/edge defects in MBE grown transition metal dichalcogenides

Cite as: APL Mater. 6, 056103 (2018); https://doi.org/10.1063/1.5022339
Submitted: 14 January 2018 . Accepted: 13 April 2018 . Published Online: 04 May 2018

Ke Chen, Anupam Roy, Amritesh Rai, Hema C. P. Movva, Xianghai Meng, Feng He, Sanjay K. Banerjee, and Yaguo Wang

Accelerated carrier recombination by grain boundary/edge defects in MBE grown transition metal dichalcogenides

Ke Chen,[1] Anupam Roy,[2] Amritesh Rai,[2] Hema C. P. Movva,[2] Xianghai Meng,[1] Feng He,[1,3] Sanjay K. Banerjee,[2] and Yaguo Wang[1,3,a]
[1]*Department of Mechanical Engineering, The University of Texas at Austin, Austin, Texas 78712, USA*
[2]*Microelectronics Research Center and Department of Electrical and Computer Engineering, The University of Texas at Austin, Austin, Texas 78758, USA*
[3]*Texas Materials Institute, The University of Texas at Austin, Austin, Texas 78712, USA*

(Received 14 January 2018; accepted 13 April 2018; published online 4 May 2018)

Defect-carrier interaction in transition metal dichalcogenides (TMDs) plays important roles in carrier relaxation dynamics and carrier transport, which determines the performance of electronic devices. With femtosecond laser time-resolved spectroscopy, we investigated the effect of grain boundary/edge defects on the ultrafast dynamics of photoexcited carrier in molecular beam epitaxy (MBE)-grown $MoTe_2$ and $MoSe_2$. We found that, comparing with exfoliated samples, the carrier recombination rate in MBE-grown samples accelerates by about 50 times. We attribute this striking difference to the existence of abundant grain boundary/edge defects in MBE-grown samples, which can serve as effective recombination centers for the photoexcited carriers. We also observed coherent acoustic phonons in both exfoliated and MBE-grown $MoTe_2$, indicating strong electron-phonon coupling in this materials. Our measured sound velocity agrees well with the previously reported result of theoretical calculation. Our findings provide a useful reference for the fundamental parameters: carrier lifetime and sound velocity and reveal the undiscovered carrier recombination effect of grain boundary/edge defects, both of which will facilitate the defect engineering in TMD materials for high speed opto-electronics. https://doi.org/10.1063/1.5022339

Transition metal dichalcogenides (TMDs), a family of layered materials, have attracted tremendous interest in recent years due to their unique properties at two-dimensional scale, such as direct bandgap in a monolayer,[1] stable exciton,[2] strong spin-valley coupling,[3] and immunity to short channel effects.[4] One potential application of TMDs is flexible nano-optoelectronics, in which the dynamics of the photoexcited carriers/excitons plays an essential role in determining the device performance and functionality. Thus, measuring and understanding the dynamics of photoexcited carriers in TMDs are very important to realize novel electronic devices. Currently, there are mainly three ways to produce 2D TMDs: mechanical exfoliation, chemical vapor deposition (CVD), and molecular beam epitaxy (MBE) growth. While the most abundant defects in all three kinds of TMDs are chalcogen vacancies, CVD and MBE TMD samples show a considerable amount of other defect species, such as grain boundary/edge (GB/E) sites and impurities.[5] Typically, defects can have significant impact on the carrier dynamics. For example, chalcogen vacancies can induce mid-gap states which can give rise to radiative bound excitons, reducing the intrinsic PL intensity.[6] While oxygen impurities occupying chalcogen vacancy sites can eliminate the mid-gap states,[7] oxygen impurities taking up molybdenum vacancy sites keep those mid-gap states and play the role as effective carrier trappers.[8,9]

Comparing with exfoliated and CVD synthesized samples, studies on the photoexcited carrier dynamics in MBE-grown TMDs are rare. Our previous work has shown that one of the main

[a]Author to whom correspondence should be addressed: yaguo.wang@austin.utexas.edu

structural defects in MBE-grown TMDs is the GB/E sites.[10] These GB/E defects can hinder the carrier transport by introducing localized charge-carrier states. However, the effect of these defects on the carrier relaxation dynamics remains unknown. In this letter, we utilize femtosecond laser pump-probe spectroscopy to investigate the photoexcited carrier dynamics in MBE-grown $MoSe_2$ and $MoTe_2$ thin films. Comparing with exfoliated samples, the excited carrier decay rates in MBE-grown samples are about 50 times faster, as revealed by transient reflection signals, which suggests that the GB/E defects in MBE samples can serve as effective recombination centers for the photoexcited electron-hole pairs. Coherent acoustic phonons in both MBE-grown and exfoliated $MoTe_2$ thin films have also been observed, from which the phonon sound velocities are extracted that agree with the theoretical value.

Hexagonal $MoSe_2$ and $MoTe_2$ thin films (2H polytype) are uniformly grown over a large area on sapphire substrates by MBE, with a thickness of 5 nm (~7 layers). Details of the growth process and the structural, spectroscopic, and electrical characterization of the samples can be found in our previous work.[10] Figures 1(a) and 1(b) show the transmission electron microscopy (TEM) images of the MBE samples.[10] The main feature of the MBE samples is the presence of a large amount of nanometer-sized grains and, thus, plenty of the GB/E sites. The origin of these small size grains is still not well known; one possible reason could be that the large vapor pressure difference between Mo and the chalcogen species adversely narrows the growth window, thereby making the film prone to chalcogen defects and reduced grain dimensions. Similar grain structures have been observed in MBE $MoSe_2$ reported by other groups.[11,12] In contrast, exfoliated TMD samples have much larger grain size and thus much fewer GB/E defects.[13–16] As shown in Fig. 1(c),[14] no obvious GB/E can be seen in exfoliated $MoSe_2$ within an area comparable to Fig. 1(b).

The large difference in the density of GB/E sites between MBE-grown and exfoliated samples provides us a good physical model to study the effect of boundary defects on the photoexcited carrier dynamics. For comparison, we have also mechanically exfoliated $MoSe_2$ and $MoTe_2$ thick flakes onto Si and sapphire substrates with a scotch tape, respectively. The thickness of the exfoliated $MoSe_2$ and $MoTe_2$ is 80 nm and 1.3 μm, respectively, measured with AFM (supplementary material). The lateral minimum dimension of the exfoliated $MoSe_2$ and $MoTe_2$ is both around 70 μm (supplementary material). We have measured the transient differential reflection signals ($\Delta R/R_0$, where R and R_0 are the reflectivities after and before the pump excitation, respectively) in both MBE-grown and exfoliated samples with femtosecond laser pump-probe spectroscopy and compared the carrier relaxation rates in these samples. Our laser pulses are generated from a Ti:sapphire oscillator operating at 80 MHz repetition rate, with about 100 fs pulse width (FWHM), 800 nm central wavelength, and 30 μm diameter of laser spots on the sample surface. Details of our experimental setup can be found in Ref. 8. Figure 2(a) shows the $\Delta R/R_0$ signals in exfoliated $MoTe_2$ measured at different pump

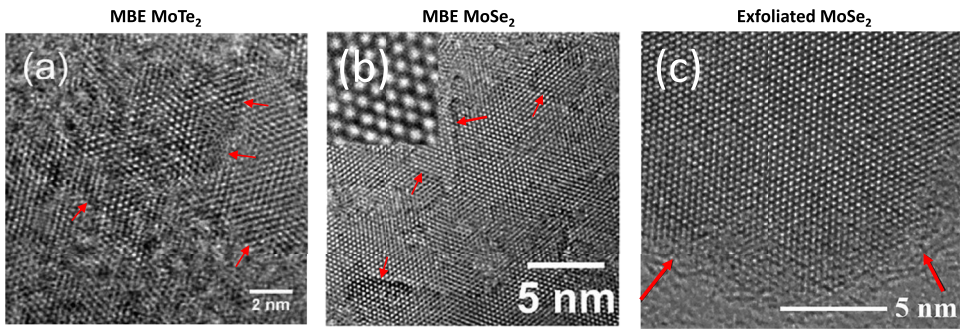

FIG. 1. [(a) and (b)] TEM images of MBE-grown $MoTe_2$ and $MoSe_2$.[10] Abundent nano-sized grains and plenty of grain boundary/edge defects are present. The arrows indicate some of the grain boundaries and edges. Reprinted with permission from Roy *et al.*, ACS Appl. Mater. Interfaces **8**(11), 7396–7402 (2016). Copyright 2016 American Chemical Society. (c) TEM images of exfoliated $MoSe_2$.[14] Very few grain boundary/edge defects can be seen. The arrows indicate the border of the exfoliated sheet. Reprinted with permission from Lei *et al.*, Small **12**(23), 3112–3118 (2016). Copyright 2016 John Wiley & Sons, Inc.

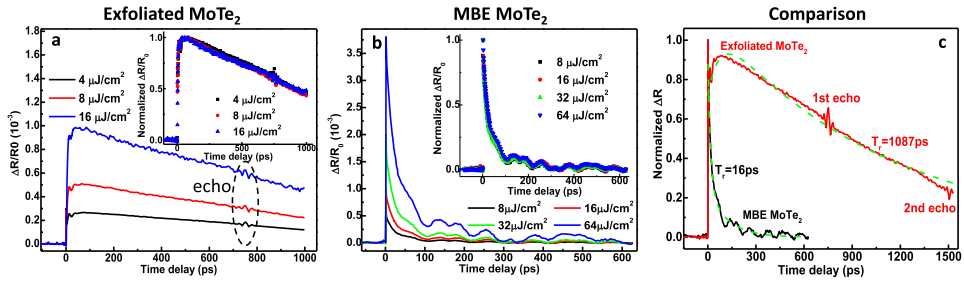

FIG. 2. (a) Differential reflection signals of exfoliated $MoTe_2$ at different pump fluences (1 μJ/cm^2 corresponding to a carrier density of 4.5×10^{17} cm^{-3}). Inset: normalized $\Delta R/R_0$ signals. (b) Differential reflection signals $\Delta R/R_0$ of MBE-grown $MoTe_2$ at different pump fluences (1 μJ/cm^2 corresponding to a carrier density of 1.3×10^{18} cm^{-3}). Inset: normalized $\Delta R/R_0$ signals. (c) Comparison of normalized $\Delta R/R_0$ signals in MBE $MoTe_2$ and exfoliated $MoTe_2$, measured at small step size with the echoes and oscillations from acoustic phonons clearly shown. Dashed curves are the fittings using Eq. (1).

fluences. Besides the sharp rise at the beginning due to the excitation, the signals consist of another small rise after the excitation and then a slow decay component. Noticeable pulse-like signals are observed at the beginning and around 750 ps later (echo), which are related to coherent acoustic phonons (strain pulse) generated by a pump laser and will be discussed later. Multilayer $MoTe_2$ has an energy difference of 1.16 eV at the K point in the momentum space.[17] In our experiment, the pump and probe photon energies are identical (around 1.55 eV), much higher than the energy gap at the K point. Therefore, after excitation, the photoexcited electrons/holes will not stay at the pumped (also probed) energy level but quickly relax to the bottom/top states of the conduction/valence band through carrier-carrier scattering (carrier thermalization process to reach a temperature-defined Fermi distribution) and carrier-phonon scattering (carrier cooling process to reach an equilibrium temperature between carrier and phonon systems), respectively.[18] During these processes, the excess energy of carriers is transferred to the phonon system, generating coherent acoustic phonons and increasing the lattice temperature. After the ultrafast (fs to ps time scale) carrier thermalization,[18] the phase space filling effect[19] at the probed energy level should be rather weak due to a very small or even no occupation at that level. Hence, unlike the resonantly probed case, the reflection change ΔR in the non-resonantly probed case here should not be sensitive to the change in absorption coefficient α (or equivalently, extinction coefficient k, the imaginary part of the complex refractive index) induced by the Pauli blocking of the phase filling effect, but should be mainly dominated by the real part of the complex reflective index change induced by the thermalized carriers instead.[9] Therefore, the small increase in $\Delta R/R_0$ signal after the sharp rise can be attributed to the refractive index change (real part) induced by a slight lattice temperature increase, and the decay of the $\Delta R/R_0$ signal actually reflects the recombination process of the thermalized electron-hole pairs. A discussion on the signal detection mechanism can be found in the supplementary material. Figure 2(a) shows that the peak of the $\Delta R/R_0$ signal is proportional to the pump fluence, and the signals measured at different pump fluences overlap when normalized (as shown in the inset), which indicates that the pump fluences used in our experiments are small enough that the $\Delta R/R_0$ value is linear with the excited carrier density.[20]

Figure 2(b) shows the transient differential $\Delta R/R_0$ signals of MBE $MoTe_2$ measured at different pump fluences. The signals are exponential decays superposed with clear periodic oscillations, which are the coherent acoustic phonons (strain pulse) generated by the pump laser and will be discussed later. Similar to that in the exfoliated sample, the decay is from the decreasing of the excited carrier density due to electron-hole pair recombination. The magnitude of $\Delta R/R_0$ signals is also proportional to the pump fluence, and the normalized signals overlap as shown in the inset, indicating that the pump fluence is low enough to ensure a linear relation between the value of $\Delta R/R_0$ signals and the excited carrier density plus the phonon vibration amplitude.[20]

The comparison of $\Delta R/R_0$ signals in exfoliated and MBE $MoTe_2$ is shown in Fig. 2(c). A gigantic difference in the signal decay rates is observed. Based on the above signal analysis, the non-oscillating

part of the transient $\Delta R/R_0$ signals (not considering the echoes and oscillations from acoustic phonons) in exfoliated and MBE $MoTe_2$ after carrier thermalization (fs to ps process) can be described with the following expression:

$$\frac{\Delta R}{R_0}(t) = A_T\left(1 - e^{-\frac{t}{\tau_{rise}}}\right)e^{-\frac{t}{\tau_c}} + A_{cool}e^{-\frac{t}{\tau_{cool}}} + A_e e^{-\frac{t}{\tau_r}}. \quad (1)$$

The first, second, and third terms on the right-hand side of Eq. (1) represent the lattice temperature change, the carrier cooling process, and the carrier recombination, respectively. A_T, A_{cool}, and A_e are the signal amplitude for lattice temperature change, carrier cooling, and carrier recombination, respectively, and τ_{rise}, τ_c, τ_{cool}, and τ_r are the time for lattice temperature rise from laser heating, the time for lattice temperature decrease due to heat conduction, the carrier cooling time, and the carrier recombination lifetime, respectively. The fitting results using Eq. (1) are shown in Fig. 2(c) as dashed lines. Detailed interpretation about the fitting procedure can be found in the supplementary material. The fitted value of carrier lifetime τ_r for exfoliated and MBE $MoTe_2$ is 1087 ps and 16 ps, respectively. Obviously, the huge difference in carrier lifetime should come from the distinction in structural properties between the two samples: either the dimension (thickness) or the structural defects. The MBE sample has a thickness of 5 nm (7 atomic layers). It has been reported that multilayer MoS_2 samples with a thickness larger than 6 atomic layers have carrier lifetimes close to that of the bulk MoS_2 sample,[21] which suggests that the difference in structural defects but not the thickness should be responsible for the observed lifetime difference here. Generally, chalcogen vacancy is the most abundant defect species in TMD materials.[22] However, we can rule out the relevance of Te vacancies to the observed reduction of carrier lifetime in the MBE sample because the densities of Te vacancies are similar in exfoliated $MoTe_2$ (Te:Mo ratio ~ 1.90:1, see the supplementary material) and MBE $MoTe_2$ (Te:Mo ratio ~ 1.91:1[10]), based on our X-ray photoelectron spectroscopy (XPS) measurements. As shown in Fig. 1, MBE TMDs have much more GB/E defects than the exfoliated one. This distinction strongly suggests that the carrier-GB/E defect interaction should account for the dramatic decrease in carrier lifetime in the MBE $MoTe_2$ sample. GB/E sites are defects in the form of the displacement of host atoms and represents structural damage to the lattice. These defects can typically introduce energy levels in the bandgap and serve as efficient recombination centers that can capture the photoexcited electrons and holes at similar rates, with the time scale usually much shorter than the intrinsic lifetime.[23] Therefore, the carrier recombination process can be accelerated by the GB/E defects, and the effective carrier lifetime is thus shortened dramatically, as demonstrated in Fig. 2(c). Previously, the defect-assisted electron-hole recombination has been observed.[24] However, the previous study could not identify a specific type of defect as the recombination center. Here, by comparing the carrier relaxation dynamics in exfoliated and MBE-grown samples with large difference in the density of specific defects, we suggest that the GB/E defects are responsible for the observed lifetime reduction in MBE-grown $MoTe_2$.

To confirm whether the recombination-center nature of GB/E defects is universal in MBE-grown TMDs, we conducted similar measurements of the differential reflection signal $\Delta R/R_0$ in exfoliated and MBE grown $MoSe_2$, as shown in Figs. 3(a) and 3(b), respectively. Bulk $MoSe_2$ has an energy gap around 1.55 eV at the K(K′) point,[10] resonant with our pump and probe photon energies. With resonant detection, the reflection change is dominated by the absorption coefficient change due to the phase-space filling effect.[8,9] For both samples (exfoliated $MoSe_2$ on the Si substrate and the $MoSe_2$ thin film grown on the sapphire substrate by MBE), the reflection change is proportional to the absorption coefficient change, according to the calculation with the transfer matrix method (supplementary material).[8,9] Thus, the response of negative reflection change ΔR means that the absorption coefficient decreases after the pump excitation, which is consistent with the Pauli blocking/repulsion induced by the phase-space filling effect. As shown in Figs. 3(a) and 3(b) and the insets, the $\Delta R/R_0$ signals are proportional to the pump fluence and overlap when normalized (at around 4 ps), suggesting that the experiments are performed in the linear region and the $\Delta R/R_0$ values are proportional to the excited carrier density at the detected energy states.[19] The sharp peaks shown in Figs. 3(a) and 3(b) are due to the carrier redistribution after excitation (carrier thermalization and carrier cooling), and the following decay mainly reflects the recombination of carriers in the K(K′) valleys.[9] Unlike $MoTe_2$, neither the

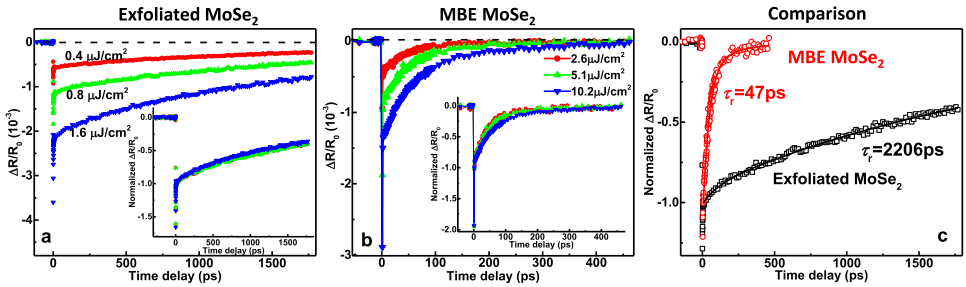

FIG. 3. (a) Differential reflection signals of exfoliated $MoSe_2$ samples at different pump fluences (1 μJ/cm^2 corresponding to a carrier density of 3.9×10^{17} cm^{-3}). Inset: normalized $\Delta R/R_0$ signals. (b) Differential reflection signals $\Delta R/R_0$ of MBE $MoSe_2$ samples at different pump fluences (1 μJ/cm^2 corresponding to a carrier density of 1.3×10^{18} cm^{-3}). Inset: normalized $\Delta R/R_0$ signals. (c) Comparison of normalized $\Delta R/R_0$ signals between MBE $MoSe_2$ and exfoliated $MoSe_2$. Solid curves are the fitting using Eq. (1).

echoes/oscillations from acoustic phonons nor significant contribution from lattice heating and heat conduction is observed in $MoSe_2$. This difference indicates that $MoTe_2$ has strong electron-phonon coupling through which the energy initially absorbed by the carrier system can rapidly transfer to the phonon system, generate coherent phonons, and lead to a detectable lattice temperature increase. The absence of coherent phonons in $MoSe_2$ is not related to the resonant probing condition because previous studies show that coherent phonons could be more prominent when probed resonantly.[25,26] It remains unclear why $MoTe_2$ has such an extraordinary electron-phonon coupling strength, but the discussion about this topic is beyond the scope of this article. With weak electron-phonon coupling considered, the $\Delta R/R_0$ signals in $MoSe_2$ samples can also be described by Eq. (1) but without the first (thermal) term. Figure 3(c) shows the comparison of the normalized $\Delta R/R_0$ signal in the exfoliated and MBE-grown $MoSe_2$ samples, along with the fittings with Eq. (1). Similar to $MoTe_2$, the signals in MBE-grown $MoSe_2$ also decay much faster than that in the exfoliated sample. The fitted carrier lifetimes are 47 ps and 2206 ps for MBE and exfoliated samples, respectively. This huge difference is also attributed to the acceleration of carrier recombination in MBE-grown $MoSe_2$ through the GB/E defects. Thus, the observation of substantially reduced lifetime in MBE-grown $MoSe_2$ again demonstrates the role of GB/E defects as efficient recombination accelerators and this role should be universal in all TMD materials.

Theoretically, the defect-capture associated carrier lifetime can be estimated with a simple model, $\tau_r = 1/v_{th}\sigma N_{def}$,[27] where v_{th} is the carrier thermal velocity, σ is the carrier capture cross section, and N_{def} is the defect density. From the TEM images of our MBE-grown samples shown in Fig. 1, it is estimated that the average grain boundary defect densities N_{def} of MBE-grown $MoSe_2$ and $MoTe_2$ are around 5×10^{26} m^{-3} and 1.7×10^{27} m^{-3}, respectively (by counting the number of defect sites and assuming each layer has similar defect density). Carrier thermal velocity in a semiconductor can be estimated as $v_{th} = \sqrt{3k_BT/m^*}$, where k_B is the Boltzmann constant, T is the temperature, and m^* is the electron effective mass, and is typically on the order of 1×10^5 m/s. The carrier capture cross section of grain boundary defects in a semiconductor is typically on the order of 1×10^{17} cm^2.[28,29] Therefore, the theoretical values of the carrier lifetimes in our MBE-grown $MoSe_2$ and $MoTe_2$ samples are estimated to be about 15 ps and 4.8 ps, respectively, agreeing with the measured carrier lifetimes τ_r in our MBE-grown $MoSe_2$ (47 ps) and $MoTe_2$ (16 ps). This agreement is other evidence that the dramatic decrease in carrier lifetime in MBE-grown TMDs is indeed from the carrier capture effect by the large amount of grain boundary defects.

The oscillations and echoes observed in $\Delta R/R_0$ signals reveal the acoustic phonon properties in $MoTe_2$. Figures 4(a) and 4(b) show the echo signal in the exfoliated sample and the oscillation signal in the MBE sample, respectively, which are obtained by subtracting the electronic and thermal parts [fitted with Eq. (1)] from the signals shown in Fig. 2(c). In the exfoliated sample [Fig. 4(a)], the initially generated coherent phonon (strain pulse) propagates deep into the sample, is reflected at the $MoTe_2$/sapphire interface, and bounces back to the surface as an echo re-detected by the probe light.[30] This process will repeat until the echo amplitude is too weak to detect. The arrival time of the 2nd

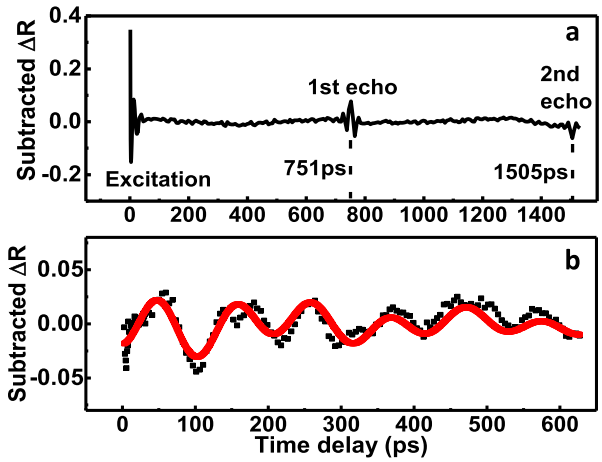

FIG. 4. (a) ΔR signal of exfoliated $MoTe_2$ with electron-background subtracted. The 1st and 2nd strain pulse echoes can be observed clearly. (b) ΔR signal of MBE-grown $MoTe_2$ with electron-background subtracted. The oscillating feature of the signal comes from the coherent acoustic phonon vibrations that modulate the refractive index of the MBE thin film. The red curve is the fitting with two damping cosine functions.

echo is just about twice of the arrival time of the 1st echo. With the measured thickness (1.3 μm), the sound velocity in exfoliated $MoTe_2$ is estimated as $v_{s_{exfo-MoTe_2}} = 2d_{exfo-MoTe_2}/T_{1st-arrive} = 3467$ m/s. The oscillations observed in the MBE sample [Fig. 4(b)] also come from the modulation of the refractive index by coherent acoustic phonons. The thickness of the MBE sample is only 5 nm, much shorter than the coherence length of the strain pulse (~350 nm, estimated from the pulse duration and the acoustic phonon velocity). The strain wave can bounce back and forth between the $MoTe_2$ surface and the $MoTe_2$/sapphire interface and form standing waves of coherent acoustic phonons, which can modulate the refractive index and thus the reflection of the probe laser. We can fit the phonon oscillations with two damping cosine functions, $\Delta R_{vib} = A_1 e^{-\frac{t}{\tau_1}} \cos(\omega_1 t + \varphi_1) + A_2 e^{-\frac{t}{\tau_2}} \cos(\omega_2 t + \varphi_2)$, where A_i, ω_i, τ_i, and φ_i are the amplitude, frequency, scattering time, and initial phase of the detected phonon modes i, respectively. The two fitted frequencies are $\omega_1 = 0.0254$ THz and $\omega_2 = 0.0596$ THz. The reason that two phonon frequencies are detected originates from the spectral response of the optical detection of phonon modes. Due to momentum conservation, the optical reflectivity detection of coherent phonons is only sensitive to the phonon modes with wave vector $q = 2k_{probe}$, where k_{probe} is the wave vector of the probe laser.[31] Even though the pump laser can generate a bunch of coherent phonon modes (there is also a spectral response for phonon generation), only the phonon modes satisfying $q = 2k_{probe}$ are scattered and detected most efficiently in our reflection signal. Along the cross-plane direction, $MoTe_2$ has two acoustic phonon dispersion curves, i.e., the longitudinal acoustic (LA) and transverse acoustic (TA) branches. Therefore, $\omega_1 = 0.0254$ THz and $\omega_2 = 0.0596$ THz are probably the TA and LA modes at $q = 2k_{probe} = 2\frac{2\pi}{\lambda_{probe}} = 1.57 \times 10^7$ l/m, respectively. Acoustic phonon group velocity is defined as $v_p = \frac{d\omega}{dq} \approx \frac{\omega}{q}$ (for small q). Thus, we can estimate the sound velocity in MBE $MoTe_2$ along the cross-plane direction from the measured frequency ω and its wave vector q of the LA mode, $v_{s_{MBE-MoTe_2}} = \frac{0.0596\,\text{THz}}{1.57\times10^7\,\text{l/m}} = 3796$ m/s. Our measured cross-plane sound velocities in exfoliated and MBE $MoTe_2$ agree well. To our best knowledge, this is the first time that the cross-plane sound velocity in $MoTe_2$ is experimentally measured by an optical technique. With first-principles calculations,[32] sound velocity along the out-of-plane direction in $MoTe_2$ is predicted to be around 2800 m/s. Considering the uncertainty of the Density functional theory (DFT) calculation on the choice of exchange-correlation functional,[32] our experimental sound velocity and the theoretical value agree with each other relatively well.

In summary, we have investigated the photoexcited carrier dynamics in exfoliated and MBE-grown $MoTe_2$ and $MoSe_2$ with ultrafast laser pump-probe spectroscopy. The comparison of the differential reflection signals between the exfoliated sample and the MBE-grown thin films reveals an increase in carrier recombination rate in MBE-grown samples by about 50 times. This drastic

difference is attributed to the existence of abundant GB/E defects in MBE-grown samples. Sound velocities along the cross-plane direction in $MoTe_2$ have been extracted from the coherent acoustic phonon signals, which agree with the theoretical calculation. Our results reveal the acceleration effect of GB/E defects on carrier recombination and provide a valuable reference about the carrier lifetime in exfoliated and MBE TMDs. The findings here have important implications for defect engineering in TMD materials, especially for applications where a short carrier lifetime is critical in determining the device response rate/working frequency, such as TMD-based fast photodetectors, fast saturable absorbers, and bipolar junction transistors working at the switching mode.

See supplementary material for 1—X-ray photoelectron spectroscopy (XPS) of exfoliated $MoTe_2$ flakes, 2—size and thickness of the exfoliated $MoSe_2$ and $MoTe_2$ Samples, 3—the relation between the change in reflection ΔR and the change in extinction coefficient Δk, and 4—signal detection mechanism in $MoTe_2$ samples (non-resonant case) and the fitting procedure.

The authors would like to acknowledge support from National Science Foundation (NASCENT, Grant No. EEC-1160494; CAREER, Grant No. CBET-1351881), Department of Energy (SBIR/STTR, Grant No. DE-SC0013178), and DOD_Army (Grant No. W911NF-16-1-0559 and MURI Grant No. W911NF-17-1-0312). The authors appreciate technical support from Omicron Company. The authors thank Dr. Tiger H. Tao and Shaoqing Zhang for the AFM measurement.

[1] K. F. Mak, C. Lee, J. Hone, J. Shan, and T. F. Heinz, Phys. Rev. Lett. **105**(13), 136805 (2010).
[2] D. Li, Z. Xiao, H. R. Golgir, L. Jiang, V. R. Singh, K. Keramatnejad, K. E. Smith, X. Hong, L. Jiang, and J. F. Silvain, Adv. Electron. Mater. **3**(7), 1600335 (2017).
[3] G. Kioseoglou, A. Hanbicki, M. Currie, A. Friedman, D. Gunlycke, and B. Jonker, Appl. Phys. Lett. **101**(22), 221907 (2012).
[4] H. Liu, A. T. Neal, and P. D. Ye, ACS Nano **6**(10), 8563–8569 (2012).
[5] Z. Lin, B. R. Carvalho, E. Kahn, R. Lv, R. Rao, H. Terrones, M. A. Pimenta, and M. Terrones, 2D Mater. **3**(2), 022002 (2016).
[6] S. Tongay, J. Suh, C. Ataca, W. Fan, A. Luce, J. S. Kang, J. Liu, C. Ko, R. Raghunathanan, and J. Zhou, Sci. Rep. **3**, 2657 (2013).
[7] W. Su, L. Jin, X. Qu, D. Huo, and L. Yang, Phys. Chem. Chem. Phys. **18**(20), 14001–14006 (2016).
[8] K. Chen, R. Ghosh, X. Meng, A. Roy, J.-S. Kim, F. He, S. C. Mason, X. Xu, J.-F. Lin, and D. Akinwande, npj 2D Mater. Appl. **1**(1), 15 (2017).
[9] K. Chen, A. Roy, A. Rai, A. Valsaraj, X. Meng, F. He, X. Xu, L. F. Register, S. Banerjee, and Y. Wang, ACS Appl. Mater. Interfaces **10**(1), 1125–1131 (2018).
[10] A. Roy, H. C. Movva, B. Satpati, K. Kim, R. Dey, A. Rai, T. Pramanik, S. Guchhait, E. Tutuc, and S. K. Banerjee, ACS Appl. Mater. Interfaces **8**(11), 7396–7402 (2016).
[11] S. Vishwanath, X. Liu, S. Rouvimov, P. C. Mende, A. Azcatl, S. McDonnell, R. M. Wallace, R. M. Feenstra, J. K. Furdyna, and D. Jena, 2D Mater. **2**(2), 024007 (2015).
[12] S. Vishwanath, S. Rouvimov, T. Orlova, X. Liu, J. K. Furdyna, D. Jena, and X. Xing, Microsc. Microanal. **20**(S3), 164–165 (2014).
[13] H. Qiu, T. Xu, Z. Wang, W. Ren, H. Nan, Z. Ni, Q. Chen, S. Yuan, F. Miao, F. Song, G. Long, Y. Shi, L. Sun, J. Wang, and X. Wang, Nat. Commun. **4**, 2642 (2013).
[14] Z. Lei, Y. Zhou, and P. Wu, Small **12**(23), 3112–3118 (2016).
[15] M. K. Jana and C. Rao, Philos. Trans. R. Soc., A **374**(2076), 20150318 (2016).
[16] Q. D. Truong, M. Kempaiah Devaraju, Y. Nakayasu, N. Tamura, Y. Sasaki, T. Tomai, and I. Honma, ACS Omega **2**(5), 2360–2367 (2017).
[17] W. Zhang, Z. Huang, W. Zhang, and Y. Li, Nano Res. **7**(12), 1731–1737 (2014).
[18] J. Shah, *Ultrafast Spectroscopy of Semiconductors and Semiconductor Nanostructures* (Springer Science & Business Media, 2013).
[19] N. Kumar, Q. Cui, F. Ceballos, D. He, Y. Wang, and H. Zhao, Phys. Rev. B **89**(12), 125427 (2014).
[20] K. Chen, N. Sheehan, F. He, X. Meng, S. C. Mason, S. R. Bank, and Y. Wang, ACS Photonics **4**(6), 1440–1446 (2017).
[21] H. Wang, C. Zhang, and F. Rana, Nano Lett. **15**(12), 8204–8210 (2015).
[22] J. Hong, Z. Hu, M. Probert, K. Li, D. Lv, X. Yang, L. Gu, N. Mao, Q. Feng, and L. Xie, Nat. Commun. **6**, 6293 (2015).
[23] S. M. Sze and K. K. Ng, *Physics of Semiconductor Devices* (John Wiley & Sons, 2006).
[24] H. Wang, C. Zhang, and F. Rana, Nano Lett. **15**(1), 339–345 (2014).
[25] W. Wu, Z. Chai, Y. Gao, D. Kong, F. He, X. Meng, and Y. Wang, Opt. Mater. Express **7**(5), 1547–1556 (2017).
[26] F. He, W. Wu, and Y. Wang, Appl. Phys. A **122**(8), 777 (2016).
[27] A. Mitonneau, A. Mircea, G. Martin, and D. Pons, Rev. Phys. Appl. **14**(10), 853–861 (1979).
[28] J. Lu and G. Rozgonyi, Appl. Phys. Lett. **91**(17), 172106 (2007).
[29] G. D. Barmparis, Y. S. Puzyrev, X.-G. Zhang, and S. T. Pantelides, Phys. Rev. B **92**(21), 214111 (2015).
[30] Y. Wang, C. Liebig, X. Xu, and R. Venkatasubramanian, Appl. Phys. Lett. **97**(8), 083103 (2010).
[31] M. Pascual-Winter, A. Fainstein, B. Jusserand, B. Perrin, and A. Lemaître, Phys. Rev. B **85**(23), 235443 (2012).
[32] D. O. Lindroth and P. Erhart, Phys. Rev. B **94**(11), 115205 (2016).